



HAL
open science

A Method for the Rapid Generation of Nonsequential Light-Response Curves of Chlorophyll Fluorescence

Joao Serôdio, Joao Ezequiel, Jörg Frommlet, Martin Laviale, Johann Lavaud

► **To cite this version:**

Joao Serôdio, Joao Ezequiel, Jörg Frommlet, Martin Laviale, Johann Lavaud. A Method for the Rapid Generation of Nonsequential Light-Response Curves of Chlorophyll Fluorescence. *Plant Physiology*, 2013, 163, pp.1089-1102. 10.1104/pp.113.225243 . hal-01096588

HAL Id: hal-01096588

<https://hal.science/hal-01096588>

Submitted on 19 Dec 2014

HAL is a multi-disciplinary open access archive for the deposit and dissemination of scientific research documents, whether they are published or not. The documents may come from teaching and research institutions in France or abroad, or from public or private research centers.

L'archive ouverte pluridisciplinaire **HAL**, est destinée au dépôt et à la diffusion de documents scientifiques de niveau recherche, publiés ou non, émanant des établissements d'enseignement et de recherche français ou étrangers, des laboratoires publics ou privés.

1 Running Head: Single pulse light curves

2

3

4 João Serôdio

5

6 Departamento de Biologia and CESAM – Centro de Estudos do Ambiente e do Mar,

7 Universidade de Aveiro, Campus de Santiago, 3810-193 Aveiro, Portugal

8 Tel: +351 234370787

9 E-mail: jserodio@ua.pt

10

11 Research area: Breakthrough Technologies

12

13 **A method for the rapid generation of non-sequential light-response curves of chlorophyll**
14 **fluorescence**

15
16
17
18
19
20

21 João Serôdio¹, João Ezequiel¹, Jörg Frommlet¹, Martin Laviale¹, Johann Lavaud²

22

23 Address: ¹Departamento de Biologia and CESAM – Centro de Estudos do Ambiente e do Mar,
24 Universidade de Aveiro, Campus de Santiago, 3810-193 Aveiro, Portugal; ²UMR 7266
25 ‘LIENSs’, CNRS-University of La Rochelle, Institute for Coastal and Environmental Research
26 (ILE), 2 rue Olympe de Gouges, 17 000 La Rochelle, France

27

28

29

30 One-sentence summary: Light-response curves of chlorophyll fluorescence are rapidly
31 generated from independent, non-sequential measurements through the combined use of
32 spatially separated beams of actinic light and fluorescence imaging.

33

34 Financial source: This work was supported by the FCT – Fundação para a Ciência e a
35 Tecnologia, through grants SFRH/BSAB/962/2009 (J.Serôdio), SFRH/BD/44860/2008 (J.
36 Ezequiel), and projects MigROS (PTDC/MAR/112473/2009; M. Laviale), SeReZoox
37 (PTDC/MAR/113962/2009; J. Frommlet), by the CNRS – Centre National de la
38 Recherche Scientifique (‘chercheurs invités’ program, J. Serôdio and J.Lavaud), and by the
39 French consortium CPER-Littoral, and the Egide/Campus France PHC Pessoa exchange
40 program (n°27377TB to J. Serôdio and J. Lavaud).

41

42 Corresponding author: João Serôdio, jserodio@ua.pt

43

44 **Abstract**

45 Light-response curves (LC) of chlorophyll fluorescence are widely used in plant physiology.
46 Most commonly, LCs are generated sequentially, exposing the same sample to a sequence of
47 distinct actinic light intensities. These measurements are not independent, as the response to
48 each new light level is affected by the light exposure history experienced during previous steps
49 of the LC, an issue particularly relevant in the case of the popular Rapid Light Curves. In this
50 work we demonstrate the proof of concept of a new method for the rapid generation of LCs
51 from non-sequential, temporally-independent fluorescence measurements. The method is based
52 on the combined use of sample illumination with digitally controlled, spatially separated beams
53 of actinic light, and of a fluorescence imaging system. It allows the generation of a whole LC,
54 including a large number of actinic light steps and adequate replication, within the time required
55 for a single measurement (therefore named 'Single Pulse Light Curve'). This method is
56 illustrated for the generation of LCs of PSII quantum yield ($\Delta F/F_m$), relative electron transport
57 rate (rETR) and non-photochemical quenching (NPQ), on intact plant leaves exhibiting distinct
58 light responses. This approach makes it also possible to easily characterize the integrated
59 dynamic light response of a sample, by combining the measurement of LCs (actinic light
60 intensity is varied while measuring time is fixed) with induction/relaxation kinetics (actinic light
61 intensity is fixed and the response is followed over time), describing both how the response to
62 light varies with time and how the response kinetics varies with light intensity.

63

64 Light-response curves (LC) are widely used in plant physiology for the
65 quantitative description of the light-dependence of photosynthetic processes (Henley, 1993).
66 Originally developed for characterizing the response of steady state photosynthesis to ambient
67 irradiance (Smith, 1936), LCs attained widespread use following the introduction of Pulse
68 Amplitude Modulated (PAM) fluorometry (Schreiber et al., 1986). Through its ability to
69 monitor the activity of photosystem II (PSII), this technique allows the generation of LCs of
70 relative electron transport rate (rETR; Schreiber et al., 1994), a non-invasive and real-time
71 indicator of photosynthetic activity, shown to be a close proxy for biomass-specific rates of
72 photosynthesis (Genty et al., 1989; Seaton and Walker, 1990). Due to the considerable
73 operational advantages of PAM fluorometry, LCs of rETR became the most common form of
74 quantitatively characterizing the light response of photosynthetic activity in plants as well as in
75 virtually all types of photoautotrophic organisms (Rascher et al., 2000; Serôdio et al., 2005; Ye
76 et al., 2012).

77 Ideally, LCs should be based on independent measurements of the parameter under study.
78 For example, in ¹⁴C-based methods of measuring photosynthetic rates in phytoplankton this is
79 the case (Johnson and Sheldon, 2007). It is also possible to generate LCs from PAM
80 measurements in independent replicated samples (Lavaud et al., 2007) but the need to cover a
81 wide range of actinic light levels with appropriate replication makes this approach very time and
82 sample consuming. Therefore, in most cases LCs are generated sequentially, by exposing the
83 same sample to a (usually increasing) range of irradiance levels (Schreiber et al., 1994).

84 An often overlooked consequence of sequential LCs is that the response of the sample
85 under each light level is strongly affected by its exposure to previous light levels (Perkins et al.,
86 2006; Herlory et al., 2007; Ihnken et al., 2010). LCs constructed in this way are therefore
87 dependent not only on the absolute light levels applied during the generation of the curve but
88 also on the duration of the exposure to each light level and on their order of application. The
89 effects of non-independency between measurements are expected to be intensified in the case of
90 rapid light curves (RLC; Schreiber et al., 1997; White and Critchley, 1999), curves generated by
91 reducing the duration of each light step, normally to just 10-30 s (Rascher et al., 2000; Ralph
92 and Gademann, 2005; Perkins et al., 2006). The short duration of the light steps do not allow the
93 sample to reach a steady state under each light level, thus being largely influenced by previous
94 light history (Serôdio et al., 2006; Ihnken et al., 2010; Lefebvre et al., 2011).

95 Here we present an alternative method to generate LCs of fluorescence parameters from
96 truly independent, non-sequential measurements. The method is based on the spatial separation
97 of the different levels of actinic light used to construct the light curve, and uses the capabilities
98 of chlorophyll fluorescence imaging systems to simultaneously measure the fluorescence
99 emitted by samples exposed to different irradiance levels. This approach enables light curves to
100 be measured very rapidly, as it only requires that the samples are exposed to the different actinic

101 light levels for the desired period of time (e.g. to reach a steady-state condition) before a single
102 saturating pulse is applied to measure the fluorescence response of all samples simultaneously.
103 By reducing significantly the time required for the generation of LCs, this approach makes it
104 possible to easily characterize the dynamic light response, by simultaneously tracing the
105 fluorescence response under different light intensities over time.

106 This work demonstrates the proof of concept for the generation of LCs through the
107 combined use of (i) sample illumination with spatially separated light beams of different
108 intensity, through the use a digital projector as a source of actinic light, and (ii)
109 imagingchlorophyll fluorometry. The application of the method is illustrated for intact plant
110 leaves, but its general principle of operation is applicable to any other type of photosynthetic
111 samples, like macroalgae, lichens or suspensions of microalgae or chloroplasts.

112

113

114 **RESULTS**

115

116 **Rationale of the method**

117 The method is based on the illumination of replicated samples with actinic light of different
118 intensities and on the simultaneous detection of the induced fluorescence by an imaging
119 chlorophyll fluorometer. The method requires a number of conditions to be met.

120 A fundamental requirement is that the illumination of the samples with different levels of
121 actinic light must not interfere with its exposure to the measuring light and saturation pulses.
122 For this reason, the best solution is to project on the samples the required combination of actinic
123 light levels ('light mask', see below) using a light source positioned from such a distance that
124 the measuring light and saturating pulses can reach the samples unimpeded. This approach also
125 allows for the measuring light and the saturating pulses to illuminate the sample while it is
126 exposed to the actinic light, a critical condition of the saturating pulse method (Schreiber et al.,
127 1986). Nonetheless, in order to be useful for the generation of a light curve, the fluorescence
128 response must be related solely to the different actinic light levels applied. This implies the use
129 of either replicated samples (e.g. microalgae culture in a multi-well plate) or a homogeneous
130 single sample (e.g. whole leaf). In the latter case, however, the independence of the
131 measurements may be compromised by light scattering within the sample (leaf tissue) causing
132 light spillover between adjacent areas illuminated with different actinic light levels (see below).
133 In this study a digital projector was used as a source of actinic light, due to the large potential
134 advantages deriving from the versatility provided by the digital control of light output.
135 However, the novelty of this approach in plant photophysiology required extensive testing both
136 regarding the emitted light and the detection of fluorescence response.

137 Regarding light output, the digital projector used in this study was analyzed concerning
138 the spectral characteristics of the emitted light. An important condition for any light source to be
139 used for generating light-response curves is that the light spectrum does not change significantly
140 over the range of light intensities applied. Otherwise, substantial distortions in the light curve
141 shape may be induced, as the photosynthetic light absorption varies significantly along the
142 different regions of the spectrum. This was tested by measuring the spectrum of light emitted at
143 the various output intensities used for generating light curves.

144 The use of a digital projector was also tested regarding the potential interference on the
145 detection of the fluorescence signals. Images produced by digital projectors are known to suffer
146 from flickering which, although imperceptible to the human eye, may affect the determination
147 of fluorescence levels F_s and F_m' and the calculation of fluorescence indices like $\Delta F/F_m'$ or
148 NPQ. Preliminary tests were made on the two main types of digital projector, LCD and DLP
149 projectors. In LCD projectors, images are generated from light beams (three, each of one
150 primary color) passing through separate LCD panels made of a large number of liquid crystals,
151 each corresponding to a pixel in the projected image. The three beams are later combined into a
152 single, full color beam. In the case of DLP technology, the projected light beam arises from
153 light reflected from a reflective surface made of a large number of small mirrors (DLP chip),
154 each corresponding to a pixel in the final image. The orientation of each mirror is controlled
155 individually determining the intensity of each pixel. The interference of actinic light flickering
156 on fluorescence measurements was tested by analyzing the fluorescence kinetics immediately
157 before (determination of F_s level) and during the application of a saturating pulse (determination
158 of F_m' level), on samples exposed to different actinic light intensities provided by the projector.
159 DLP projectors exhibited a much higher intensity of flickering, making them impossible to use
160 in this context. The study was thus carried out using a LCD projector (see below).

161 162 **Actinic light spectrum**

163 The spectrum of the light emitted by the digital projector covered the wavelength range of
164 PAR, from ca. 430 nm to over 700 nm (Fig. 2A). The projected light was rich in
165 photosynthetically active blue light, its spectrum showing a distinct peak at 440 nm, but poorer
166 in red light (650-700 nm band). The spectrum showed two large peaks in the green-yellow
167 region, centered at 550 and 580 nm. Very little thermal radiation (above 750 nm) was emitted,
168 even when applying the highest PAR levels. This means that the used projector was a suitable
169 source of cold actinic light, which did not induce differences in temperature over the different
170 AALs.

171 The light spectrum was found to change substantially when varying the lamp output
172 intensity (Fig. 2B). Below moderate PAR values (e.g. $580 \mu\text{mol m}^{-2} \text{s}^{-1}$ at the sample level),
173 irradiance increased equally over most of the spectral range (flat spectrum from 440 to 675 nm;

174 when compared to $150 \mu\text{mol m}^{-2} \text{s}^{-1}$). But for higher lamp outputs (e.g. $1125 \mu\text{mol m}^{-2} \text{s}^{-1}$), the
175 spectrum was increasingly enriched in green-yellow light (mainly green, 525-590 nm, and
176 yellow-orange, 600-660 nm) becoming comparatively poorer in photosynthetically active blue
177 and red light. The variation of the light spectrum with intensity may represent a major problem
178 for the generation of light-response curves. Because the yellow-green light that dominates the
179 spectrum when applying higher light levels is poorly absorbed by photosynthetic pigments, the
180 corresponding values of $\Delta F/F_m'$ (or rETR) will appear overestimated when plotted against the
181 measured PAR levels. As a result, rETR/light-response curves may show an inflexion in the
182 light-saturated region, showing an increase of rETR values when stabilization or even a decrease
183 would be expected.

184 This problem was addressed by manipulating the spectrum of emitted light so that the
185 proportions of red, green and blue (RGB ratio) regions of the spectrum remained approximately
186 constant over the whole range of light intensities applied. This was achieved through an iterative
187 process of changing the MS Visual Basic code controlling the RGB ratio of the images produced
188 by the projector, measuring the emitted spectrum, and calculating the resulting proportions of
189 red, green and blue spectral regions. The RGB code allowed to independently control the
190 spectral ranges of 400-486 (blue), 487-589 (green-yellow) and 590-690 (red) nm. This procedure
191 was repeated until the same proportions of RGB were obtained in the emitted light for the
192 various PAR levels that were used for generating light-response curves. An average proportion
193 R:G:B of 0.7:2.2:1 was used (Fig. 2C), which, by having a higher proportion of yellow-green
194 light ensured the emission of high maximum PAR levels ($1125 \mu\text{mol m}^{-2} \text{s}^{-1}$ at the sample
195 level).

196

197 **Actinic light flickering**

198 The projector light showed noticeable flickering, causing obvious fluctuations in the
199 fluorescence trace (Fig. 3). Light flickering caused interferences at 1.8 s intervals, more
200 pronounced under higher actinic light levels, when it significantly affected the correct
201 determination of both F_s and F_m' levels. Using the data of Fig. 3 as an example, if the full
202 fluorescence record was considered for calculating F_s and F_m' , it would result in an
203 underestimation of $\Delta F/F_m'$ values of 3.0% and 22.3%, for 260 and $850 \mu\text{mol m}^{-2} \text{s}^{-1}$,
204 respectively. To avoid these confounding effects it was necessary to analyze the fluorescence
205 recording for each individual measurement (immediately before and during a saturating pulse)
206 and exclude the affected data points.

207

208 **Application to intact leaves**

209 The method was tested on intact leaves of plants acclimated to different light regimes,
210 expected to show contrasting features in light-response curves of fluorescence. Figure 4 shows

211 chlorophyll fluorescence images resulting from the application of an actinic light mask to leaves
212 of HL-acclimated *Hedera helix* (Fig. 4A-C) and LL-acclimated *Ficus benjamina* (Fig. 4D-F) for
213 a known period of time.

214 Images of F_s and F_m' of *H. helix* (Fig. 4A,B) showed some degree of heterogeneity, with
215 higher absolute pixel values in the central region of the leaf, and lower values in the extremities.
216 This was due to the large leaf size in relation to the projected light fields of measuring light and
217 saturating pulses. However, this did not affect significantly the determination of the ratio
218 $\Delta F/F_m'$, which remained relatively constant throughout the whole leaf (varying between 0.79
219 and 0.83; Fig. 4C). In the case of *F. benjamina*, although the smaller leaf size helped reduce the
220 effects of light field heterogeneity, spatial variability was still noticeable due to certain leaf
221 anatomical features (e.g. central vein). Again, while this was evident for F_s and F_m' images, the
222 effect mostly disappeared when the ratio $\Delta F/F_m'$ was calculated (Fig. 4F).

223 The application of the actinic light mask on intact leaves resulted in well-defined areas of
224 induced fluorescence response. Particularly for higher light levels, each AAL showed a
225 noticeable outer ring of pixels of intensity intermediate between background values (not
226 illuminated areas) and fully illuminated areas (center of each AAL). The resulting fluorescence
227 images showed a clearly different pattern of response to actinic light in the two plants. Whilst
228 for the HL-acclimated *H. helix*, little effects were observed on F_s , which remained virtually
229 constant over the range of PAR levels applied (Fig. 4A), for the LL-acclimated *F. benjamina*, a
230 large variation in F_s was observed (Fig. 4D). Also regarding F_m' , it was clear that in *H. helix* the
231 exposure to high light caused a larger decrease than in *F. benjamina*. As a consequence, clear
232 differences were also observed regarding $\Delta F/F_m'$ values, which reached lower values in the LL-
233 acclimated plant. It may be noted that there was a high similarity between replicated AAL and
234 that, as in the case of *F. benjamina*, heterogeneities in F_s and F_m' had little effect on $\Delta F/F_m'$
235 (Fig. 4D-F).

236 These fluorescence images are also useful to illustrate the variability regarding light
237 scattering within the leaf and its impact on the applicability of the method to intact leaves. *H.*
238 *helix* leaves showed very low spillover between adjacent AAL, as deduced from the similarity
239 between the pixel values of the areas between AALs and of the background (parts of the leaf
240 distant from AALs; Fig. 4B,C). Notably, larger spillover effects were observed in the lower
241 (abaxial) surface of the *H. helix* leaves (data not shown). In contrast with *H. helix*, leaves of *F.*
242 *benjamina* showed a much larger light spillover around AALs. Both for F_s and F_m' , the areas
243 around AALs showed pixel values clearly different from the background values (Fig. 4D, E).
244 However, this did not seem to affect significantly the determination of F_s , F_m' or $\Delta F/F_m'$ in each
245 AOI, as no asymmetry was evident in pixel intensity within the AOI of the mask's outer arrays.

246

247 **Light-response curves: 'Single Pulse Light Curves'**

248 After defining AOIs matching the projected AALs (Fig. 4), the values of F_s and F_m' were
249 determined for the various actinic light levels. These values were used to calculate indices
250 $\Delta F/F_m'$, rETR and NPQ that, when plotted against incident actinic light, resulted in light-
251 response curves (Fig. 5). These 'Single Pulse Light Curves' (SPLC), despite requiring just a few
252 minutes of light mask exposure and a single saturating pulse, nevertheless allowed to
253 characterize in detail the light response of the tested samples. Strong indications of the quality
254 of these light curves were the low variability between replicates (measurements on AALs of
255 identical PAR level, corresponding to a same row of the light mask), and the very good fit
256 obtained with well-established mathematical models for describing rETR and NPQ vs E curves.
257 The light-response patterns were consistent with the ones expected for LL- and HL-acclimation
258 states. Departing from similar F_v/F_m values, $\Delta F/F_m'$ decreased more steeply with increasing
259 irradiance in LL-acclimated *F. benjamina* than in HL-acclimated *H. helix* (Fig. 5B, E). This
260 resulted in distinct rETR vs E curves, with *H. helix* showing higher values for initial slope (α)
261 and, mainly, maximum rETR (rETR_m, ca. 5 times higher than for *F. benjamina*). Also typical of
262 the difference between LL- and HL-acclimated samples, the photoacclimation index E_k was
263 much higher (more than double) in *H. helix* than in *F. benjamina*, in accordance with the fact
264 that the former showed little signs of saturation even at $1125 \mu\text{mol m}^{-2} \text{s}^{-1}$, while the
265 latter saturated at comparatively lower PAR values (Fig. 5E). Also in the case of NPQ vs E curves,
266 the results were in agreement with expected LL- and HL-acclimation patterns, with *H. helix*
267 reaching higher maximum NPQ values (NPQ_m), requiring higher light levels for full
268 development (E_{50}) and higher sigmoidicity (n).

269

270 **Dynamic light response**

271 A further application of the method concerns the study of the temporal variation of the light
272 response. Figure 6 shows an example of the variation over time of $\Delta F/F_m'$, rETR and NPQ for *H.*
273 *helix* and *F. benjamina* during light induction under different PAR levels. Confirming the very
274 different light-response patterns observed before, this approach made it possible to additionally
275 compare the temporal variation of the response of each fluorescence index. For the HL-
276 acclimated *H. helix*, $\Delta F/F_m'$ and rETR stabilized quite rapidly, reaching a steady state within 4-
277 6 min upon light exposure (Fig. 6A,C). The patterns of variation were essentially the same for
278 the different light levels, although stabilization was faster for the samples exposed to lower
279 PAR. For NPQ, steady state was reached only after 8-10 min, the induction pattern varying with
280 the light level applied (Fig. 6E). In the case of LL-acclimated *F. benjamina*, all indices took a
281 longer time to reach a steady state (Fig. 6 B,D,F). This was especially true for NPQ, which still
282 increased for most of the PAR levels after 14 min of light exposure.

283 This approach is also particularly useful to follow the changes in the light-response curve
284 and to determine the time necessary for reaching of a steady-state. This can be achieved by

285 following the variation over time of the model parameters used to describe the light-response
286 curves. Using the dataset partially shown on Fig. 6, Fig. 7 shows the variation during light
287 induction of the parameters of rETR and NPQ vs E curves. Regarding the rETR vs E curves, α was
288 the parameter that showed a smaller variation over time, increasing modestly until reaching
289 stable values after 6 and 10 min for *H. helix* and *F. benjamina*, respectively (Fig. 7A). In
290 contrast, rETR_m and E_k showed much larger fluctuations, particularly for *H. helix*, requiring
291 more than 8-10 min for reaching relatively stable values (Fig. 7B, C). For the parameters of
292 NPQ vs E curves, similar time periods of 6-10 min were necessary for reaching steady state
293 conditions (Fig. 7 D-F). However, despite the different induction patterns observed for HL- and
294 LL-acclimated samples, most of the differences observed at steady state were already present at
295 the first measurements (2-4 min). This indicates that even a short 2-4 min period of light mask
296 exposure may be sufficient to characterize LCs and detect differences between different light
297 acclimation states.

298

299 **Light stress-recovery experiments and NPQ components**

300 This approach can be easily extended to carry out light stress-recovery experiments, in which
301 samples are sequentially exposed to high light and then to darkness or low light, and the
302 fluorescence kinetics during light induction and dark relaxation is used to evaluate the operation
303 of photoprotective and photoinhibitory processes (Walters and Horton, 1991; Müller et al.,
304 2001). Usually, only one light level is used, of arbitrarily chosen intensity (Roháček, 2010;
305 Serôdio et al., 2012). By applying a light mask conveying a range of actinic light it becomes
306 possible to study the fluorescence kinetics during light induction and dark relaxation for
307 different PAR intensities simultaneously.

308 This is exemplified with the response of NPQ of LL-acclimated *F. benjamina* during light
309 induction and subsequent dark relaxation (Fig. 8). A large and detailed dataset was obtained
310 from a single leaf on the NPQ induction under various PAR levels (Fig. 8A, B) and on its
311 relaxation in the dark (Fig. 8C, D). Figure 8 also highlights the two types of information that
312 can be extracted from the same dataset: light-response curves (Fig. 8A, C) and
313 induction/relaxation kinetics (Fig. 8B, D). By applying the rationale used for the calculation of
314 NPQ components, such a dataset can be used to generate light-response curves of coefficients
315 quantifying photoprotection capacity and susceptibility to photoinhibition (Guadagno et al.,
316 2010). Figure 9 illustrates this approach by comparing the repartition of absorbed light energy in
317 HL-acclimated *H. helix* and LL-acclimated *F. benjamina*. The former plant was shown to be
318 able to use a larger fraction of absorbed light for photochemistry ($\Delta F/F_m'$; ca. 0.5 above 800
319 $\mu\text{mol m}^{-2} \text{s}^{-1}$; Fig. 9A) while non-photoprotective NPQ components (qT+qI) remained under
320 relatively low values (< 20%) and only started above 400 $\mu\text{mol m}^{-2} \text{s}^{-1}$ (Fig. 9A). In contrast, for
321 the LL-acclimated *F. benjamina* $\Delta F/F_m'$ was much lower throughout the light intensity range

322 (<0.2 for PAR as low as $400 \mu\text{mol m}^{-2} \text{s}^{-1}$; Fig. 9B) and NPQ started to increase under much
323 lower PAR levels, reaching maximum values at ca. $200 \mu\text{mol m}^{-2} \text{s}^{-1}$ (q_T+q_I , q_C).

324

325

326 **DISCUSSION**

327

328 **Method assumptions**

329 The purpose of this study was to demonstrate the proof of principle of the method, starting
330 by identifying and testing the conditions required for its general application. The successful
331 generation of non-sequential LCs using the combination of spatially separated actinic light
332 beams and imaging chlorophyll fluorescence implied the verification of two types of
333 assumptions: (i) assumptions associated to the projection of an actinic light mask and the
334 detection of the induced fluorescence response, and (ii) assumptions related to the use of a
335 digital projector as a source of actinic light for this purpose. These conditions were tested and
336 shown to be verified.

337 Regarding the projection of the actinic light mask, a very basic assumption of the method
338 was that the samples exposed to different actinic light levels must have essentially the same
339 inherent physiological light response, so that the fluorescence measured in different AALs may
340 be attributed to the different PAR irradiances applied. In a way, this approach is opposed to the
341 traditional use of chlorophyll fluorescence imaging systems: instead of applying a homogeneous
342 actinic light field to study heterogeneous samples, here a heterogeneous actinic light field is
343 applied to study supposedly homogeneous samples. The verification of this condition is mostly
344 dependent of the physiological heterogeneity on the samples. In some cases, as for suspensions
345 of microalgae or chloroplasts, samples can be prepared so that a uniform response can be
346 assured. However, in the case of leaves, it must be previously confirmed that the area to be used
347 for the measurements is homogeneous regarding its photophysiological responses. The here
348 presented results showed that the method can be successfully applied to whole leaves, through
349 careful selection of uniform areas, in order to minimize the potentially confounding effects of
350 within-leaf spatial inhomogeneity.

351 Another key assumption of the method is the independence of the measurements. This
352 condition can be easily ensured by using optically separated samples, using cell or chloroplast
353 suspensions, or leaf disks in opaque multi well plates impeding the transmission of light
354 between adjacent samples. Potential problems are thus restricted to optically continuous
355 samples such as whole leaves, where light spillover from one AAL to another may result in a
356 lack of independence between adjacent AAL. This effect is analogue to the time dependency
357 between consecutive measurements during a sequential light curve. The results of the tests
358 performed on leaves showed that this effect varied with species and with the leaf optical

359 properties affecting the amount of internal light scattering. However, they also showed that light
360 spillover can be greatly minimized through adequate design of the actinic light mask (see
361 below).

362 Regarding the use of digital projectors as actinic light sources, two conditions appeared to
363 be of most importance: the maintenance of a constant spectrum throughout the range of applied
364 irradiances, and the elimination of effects of light flickering on fluorescence measurements. The
365 maintenance of a constant spectrum is important because changes of light spectrum can have
366 substantial effects on $\Delta F/F_m'$, due to the variation of photosynthetic pigments absorptivity over
367 different wavelength ranges. This effect may be observed when comparing rETR light response
368 curves induced by monochromatic light of different colors (Schreiber et al., 2012). In the
369 present case, the enrichment of the green-yellow part of the spectrum is expected to cause and
370 overestimation of $\Delta F/F_m'$, for the measured PAR, because light of these wavelengths are
371 comparatively less absorbed by the dominating pigments such as chlorophyll *a* and *b*, thus
372 inducing a smaller quenching of F_s and F_m' . Therefore, if the light spectrum varies between
373 different AALs, this will likely result in a deformation of the shape of the LC, resulting in an
374 artifactual absence of saturation or decline under high light. As shown here, this problem may be
375 tackled by digitally manipulating the spectrum of the emitted light. Despite some limitations, as
376 only the spectral ranges corresponding to the RGB coding can be manipulated, this approach
377 was shown to suffice to solve the effects of the changes in lamp output spectrum. Nevertheless,
378 the need for this corrective procedure will depend on the magnitude of the induced effects, in
379 turn dependent on the particular experimental and equipment conditions such as projector and
380 lamp type, and PAR levels to be used.

381 The elimination of effects of light flickering is important because light flickering was
382 shown to cause substantial interferences in the fluorescence record, particularly for high actinic
383 light levels, under which the difference between F_s and F_m' is smaller and the error associated to
384 the determination of $\Delta F/F_m'$ is higher. While affected fluorescence values may be easily
385 identified and eliminated from the calculation of F_s and F_m' , this requires the possibility to
386 access the raw fluorescence data, which may not be feasible with some PAM fluorometer
387 models or software.

388

389 **Light mask design**

390 A crucial piece of the proposed experimental approach is the actinic light mask used to
391 project spatially separated areas of actinic light. The light mask used in this study resulted from
392 a large number of preliminary tests on several aspects such as mask shape and dimension, as
393 well as number, size and disposition of the AALs. Its development followed some principles of
394 general applicability in designing light masks for similar studies:

395 i) Mask dimension. The shape and size of the light mask should consider the sample
396 dimensions as well as the homogeneity of the measuring light and saturating pulse light fields.
397 Smaller masks likely fit better within the zone of homogenous light field sampling area, while
398 they may also help to avoid heterogeneous parts of the sample (e.g. major leaf veins). On the
399 other hand, too small masks may limit both the total number and size of AALs, and, by
400 implying short distances between adjacent AALs, may increase light spillover and compromise
401 the independency of the measurements.

402 ii) Number of AALs. A large number of AALs allows for a large number of light levels,
403 which is useful for a good characterization of the light response, and for replication, reducing
404 variability and increasing precision of parameter estimation. However, the number of AALs
405 possible to accommodate will be limited by total mask size and by the spillover between
406 adjacent AALs. In the present study, it was possible to accommodate 30 AALs, which resulted
407 in a satisfactory number of data points along the light curve and a good level of replication. By
408 effectively impeding light spillover (e.g. using opaque multi well plates), this number could be
409 significantly increased without increasing light mask size.

410 iii) AAL distribution pattern. In principle, AALs should be randomly distributed
411 throughout the light mask. This would minimize any systematic effects due to the AAL position
412 within the possibly inhomogeneous measuring light and saturating pulses fields. However, when
413 spillover effects cannot be completely avoided as in the case of whole leaves, better results were
414 found by arranging the AAL along a gradient of light intensity because in a randomized layout
415 there is a high chance of having adjacent AAL of very different light intensities, resulting in
416 substantial spillover and loss of measurement independency. When AALs are distributed along
417 a light intensity gradient, the light intensity of adjacent AALs will be more similar, thus reducing
418 the relative impact on each other. Besides preventing optical spillover, this design will also
419 minimize the potential exchange of light-induced metabolites between adjacent AALs, which
420 could contribute to some degree of non-independency between measurements, especially during
421 long light exposures, as for the study of dynamic light responses (see below). Although this
422 source of measurement dependency cannot be completely excluded for optically continuous
423 samples, its actual interference on the resulting light-response curve can be minimized by
424 decreasing the difference in light levels between AALs next to each other.

425 iv) AAL size. Large AALs should be used because more pixels will be considered for the
426 estimation of fluorescence parameters, therefore reducing measuring errors. This can be of value
427 in the case of samples showing a high physiological heterogeneity. Large AAL are also
428 preferable because the actual area used for calculation of fluorescence parameters (AOI) must
429 be smaller than the maximum diameter of AAL, to avoid the border effects. The light mask used
430 in this study had AALs of the same size and shape, disposed in linear arrays. However, masks
431 may have AAL of different size or shape and arranged in any other way, to better fit specific

432 aspects of the sample or sample container. For instance, because under higher actinic irradiances
433 a larger error is associated to the measurement of $\Delta F/F_m'$, AAL of higher light levels could be
434 larger, resulting in more precise measurements due to the higher pixel number.

435

436 **Single Pulse Light Curves**

437 The here proposed method for the generation of light-response curves presents a number of
438 innovations and significant advantages relatively to conventional approaches. It enables to: (i)
439 obtain non-sequential, temporally-independent fluorescence measurements; (ii) apply a large
440 and variable number of actinic light levels with adequate replication; (iii) generate a whole LC
441 within the time required for a single measurement; (iv) define and control with unprecedented
442 flexibility and ease of use the actinic light levels to be applied.

443 The considerable reduction of the total time required for the generation of a LC is one of
444 the major advantages of this approach. As all light levels and replicates are measured
445 simultaneously, the total duration of the LC will be essentially determined by the time defined
446 for each individual measurement (e.g. for reaching a steady-state), independently of the number
447 of light levels and replicates. For example, for the case shown in Fig. 5, the whole LC, consisting
448 of 30 measurements (10 light levels x 3 replicates), could be finished after 6 min of light
449 exposure, while it would have required a minimum of 3 hours if each light level/sample was
450 measured separately. This possibility is particularly useful when studying samples showing fast
451 changes in their physiological state, as a response to stressors or changing environmental
452 conditions, or associated to circadian rhythms (Rascher, 2001).

453 It is generally desirable for LCs to describe steady-state conditions. 'Steady-state light
454 curves' are largely independent from transient responses due to recent light history, making it
455 easier to characterize the inherent physiological light response of a sample and to compare
456 different samples. For the samples tested in this study, periods of 4-6 minutes of light mask
457 exposure were enough to ensure a good characterization of the light response, allowing the
458 estimating LC parameters and detecting differences in photoacclimation state. However, the
459 time necessary to reach steady-state conditions depends greatly on the sample physiological
460 state and previous light history. Also, because it is not likely that a steady state is reached at the
461 same time for all actinic light levels, it is not possible to define a unique protocol for the
462 application of the SPLC. Its application to samples of unknown physiological response should
463 be preceded by the preliminary monitoring of the variation over time of the fluorescence
464 response under the different actinic light levels.

465

466 **Dynamic light response**

467 The proposed method also enables to incorporate time in the study of the light response.
468 The variation over time of fluorescence indices such as $\Delta F/F_m'$, rETR or NPQ, like their light

469 induction and dark relaxation kinetics, is of obvious interest for the characterization of the
470 photophysiology of a sample. However, the patterns of variation during induction or relaxation
471 strongly depend on the level of actinic light applied. In this context, the possibility to follow the
472 response to various actinic light levels simultaneously saves time, making it considerably easier
473 to study the variation over time of the light response. This approach allows to combine two types
474 of studies that are often carried out separately: (i) light-response curves, in which actinic light
475 intensity is varied while the time for measuring a response is arbitrarily fixed; (ii)
476 induction/relaxation kinetics, in which actinic light intensity is arbitrarily fixed and the response
477 is followed over time. It becomes thus possible to easily characterize the dynamic light response
478 of a sample, describing both how the response to light varies with time and how the response
479 kinetics varies with light.

480 An application of this possibility is the construction of light-response curves of fluorescence
481 indices that require the comparison of measurements made at different times. This is the case of
482 the coefficients that quantify the partitioning of non-photochemical quenching in
483 photoprotective (rapidly reversible) and photoinhibitory (slowly reversible) components. In
484 most studies, these components are quantified for a single level of actinic light, usually
485 arbitrarily defined to represent a stressful condition. By applying the proposed method, it
486 became possible to easily generate light-response curves of the various quenching coefficients, a
487 task that requires following the NPQ relaxation kinetics after the exposure to various actinic
488 light levels, and that would otherwise be very time consuming.

489

490 **Limitations**

491 Despite the considerable advantages the here described method offers, there are a number
492 of potential limitations that must be considered. Although the results here presented are specific
493 to the particular projector model used, these general limitations are likely applicable to any
494 other models that share the same technology.

495 One limitation regards the range of actinic light levels possible to apply. On one hand, it
496 was not possible to obtain complete darkness, the minimum light intensity in the 'dark' AALs
497 being $5 \mu\text{mol m}^{-2} \text{s}^{-1}$. This was due both to the limitations of the projector's output contrast and
498 to the unavoidable light scattering originating from the illuminated areas. While this makes it
499 impossible to measure parameters that require dark adaptation, like F_o and F_m , with the
500 projector turned on, it does not affect significantly the construction of LCs, as $5 \mu\text{mol m}^{-2} \text{s}^{-1}$ can
501 be considered sufficiently low for most applications. For the special case of NPQ vs E curves,
502 which require the measurement of F_m (in the dark), the best alternative is to cover the projector's
503 lens, and determine F_m before the LC is started.

504 On the other hand, the maximum light intensity reached at the samples level may also
505 represent a limitation for the construction of LCs. In the case of the setup used in this study, the

506 maximum value of $1125 \mu\text{mol m}^{-2} \text{s}^{-1}$ can be considered low when compared to the values
507 reached by many commonly used PAM fluorometers, including imaging systems, generally
508 reaching values above $2000 \mu\text{mol m}^{-2} \text{s}^{-1}$. Nevertheless, the actual limitation caused by the
509 maximum light output will depend on the capacity to cover the relevant range of light intensities
510 for each particular sample. For the plants used in this study, the range of actinic irradiances
511 applied enabled to characterize with adequate detail the light response of the various
512 fluorescence parameters and indices, including the light-saturated part of the curve.

513 Another potential limitation derives from the relative low sensitivity of imaging
514 chlorophyll fluorometers. These imaging systems are based on CCD sensors which are less
515 sensitive than photodiodes or photomultipliers that equip the most common types of PAM
516 fluorometers. This limits the detection of fluorescence signals, especially under high actinic
517 light, when F_m' is lower and more difficult to discriminate from the F_s level. Accordingly, some
518 manufacturers do not recommend measuring LCs with PAR levels above $700 \mu\text{mol m}^{-2} \text{s}^{-1}$
519 (Imaging-PAM, 2009). This low sensitivity is expected to be overcome by using samples with a
520 high chlorophyll *a* content, but may limit the use of dilute microalgae or chloroplast
521 suspensions.

522

523 **Further applications**

524 This study aimed to show the main and most immediate applications of the method. Its use
525 was illustrated on intact plant leaves, but it is potentially applicable to many other types of
526 photosynthetic samples, ranging from large plant leaves, lichens, flat corals, macroalgae or algal
527 biofilms (microphytobenthos, periphyton) to phytoplankton or suspensions of microalgae,
528 chloroplasts or thylakoid suspensions, the main limitation being the chlorophyll *a* concentration.
529 The use of optically separated samples, as in multi-well plates, is advantageous because it
530 eliminates light spillover effects and ensures the independence of the measurements.

531 The results shown here were obtained using light masks with AALs that only differed
532 regarding light intensity. However, the digital control of actinic light opens other possibilities.
533 One is to manipulate the duration of light exposure so that in the same experiment, replicated
534 samples are exposed to different light doses, given by different combinations of light intensity
535 and exposure duration. Also color may in principle be digitally manipulated and light masks
536 made to incorporate AALs of different spectral composition. This would enable the possibility
537 to compare the spectral responses of fluorescence indices.

538 A major result of this study is the introduction of digitally controlled illumination as source
539 of actinic light for photophysiological studies involving PAM fluorometry. It provides
540 unprecedented flexibility in the control of the various aspects of projected actinic light field. As
541 this study showed, commercially-available models of digital projectors, used in combination
542 with commonly-available software, may provide a readily accessible and inexpensive way of

543 applying actinic light mask and generating SPLCs. However, such models were not built for this
544 purpose and their correct use requires some adaptations, namely regarding image flickering and
545 changes in light spectrum. We hope that this study may serve as guidelines for overcoming the
546 limitations of currently available projectors, and to stimulate the development of dedicated
547 equipment.

548

549

550 MATERIAL AND METHODS

551

552 Experimental Setup

553 The setup was comprised of a combination of a Pulse Amplitude Modulation (PAM)
554 imaging chlorophyll fluorometer and a digital projector, used as actinic light source (Fig.1). The
555 projector was positioned near the fluorometer's CCD camera, in such a way that the projected
556 light incident on the center of the area monitored by the fluorometer's camera (sampling area),
557 optimizing the detection of the induced chlorophyll fluorescence. The projector was also
558 positioned as vertically as possible (angle of 10° from vertical), to minimize asymmetries in the
559 projected light field, and as close as possible to the sample (ca. 40 cm from the projector lens to
560 the center of the sampling area), to maximize light intensity at the sample level.

561

562 Imaging chlorophyll fluorometer

563 The imaging chlorophyll fluorometer (Open FluorCAM 800-O/1010, Photon Systems
564 Instruments; Brno, Czech Republic) comprised four 13 x 13 cm LED panels emitting red light
565 (emission peak at 621 nm, 40 nm bandwidth) and a 2/3" CCD camera (CCD381) with an F1.2
566 (2.8-6 mm) objective. Two of the LED panels provided modulated measuring light ($< 0.1 \mu\text{mol}$
567 $\text{m}^{-2} \text{s}^{-1}$), and the other two provided saturating pulses ($> 7500 \mu\text{mol m}^{-2} \text{s}^{-1}$, 0.8 s). Chlorophyll
568 fluorescence images (512 x 512 pixels, 695-780 nm spectral range) were captured and processed
569 using the FluorCam7 software (Photon Systems Instruments; Brno, Czech Republic). When
570 measuring long sequences of fluorescence images (dynamic light response, see below), the
571 Fluorcam7 software was controlled by a AutoHotkey (version 1.1.09.00; available at
572 www.autohotkey.com) script written to automatically run the protocol used for applying
573 saturating pulses, save the fluorescence kinetics data for each measurement and export data as
574 text files for further processing.

575

576 Digital projector

577 All presented results were obtained using a LCD digital projector (EMP-1715, Epson,
578 Japan), comprising a mercury arc lamp providing a light output of 2700 lumens. A focusing lens
579 was used to focus the projected images in the fluorometer's sampling area. The projected light
580 field covered a rectangular area of ca. 14 x 10 cm. Projector settings were set to provide the
581 widest range of light intensities at the sample level. With the above described setup
582 configuration, PAR levels in the sampling area ranged between 5 and $1125 \mu\text{mol m}^{-2} \text{s}^{-1}$. Actinic
583 PAR irradiance at the sample level was measured using a PAR microsensor (US-SQS/W, Walz;
584 Effeltrich, Germany), calibrated against a recently-calibrated flat PAR quantum sensor (MQ-
585 200, Apogee Instruments; Logan, Utah, USA).

586

587 **Actinic light mask**

588 The digital projector was used to project an actinic light mask on the sampling area,
589 consisting of a set of spatially separated actinic light areas (AAL), covering the range of PAR
590 levels necessary to induce the fluorescence responses to be used to generate a light curve. The
591 actinic light mask used in this study consisted of 30 circular AAL arranged in a 3 x 10 matrix, in
592 which each array of 10 AAL corresponded to 10 different PAR values ($5-1125 \mu\text{mol m}^{-2} \text{s}^{-1}$),
593 arranged increasingly so that the highest values were closer to the projector (Fig. 1). Each AAL
594 consisted of a circular homogeneous light field of 4 mm in diameter. Adjacent AALs of the
595 same array were separated by 1.0 mm. Three 10-AAL arrays were projected in parallel (1.5 mm
596 apart) so that approximately the same light levels were applied on the three arrays. However, due
597 to some unavoidable degree of heterogeneity in the projected light field, a small variation (on
598 average < 2.5%) was presented among replicated AALs.

599 The light mask was designed in MS PowerPoint, using a code written in MS Visual Basic
600 to define the number, position, size and shape (slightly oval to compensate for the inclination of
601 the projector) of each AAL, as well as the light intensity and spectrum (through controlling the
602 RGB code, see below). This code was used to automatically control the PAR level of each
603 AAL, based on a relationship established between RGB settings and the PAR measured at the
604 sample level.

605 The chlorophyll fluorescence emitted at each AAL was measured by defining Areas of
606 Interest (AOI) using the FluorCam7 software. The AOIs were centered on the AALs but had a
607 smaller diameter (ca. 3 mm) to minimize border effects that could otherwise introduce
608 significant errors. On average each AOI consisted of 32 pixels.

609

610 **Actinic light spectrum**

611 The spectrum of the light emitted by the digital projector was measured over a 350-1000
612 nm bandwidth with a spectral resolution of 0.38 nm, using a USB2000 spectrometer (USB2000-
613 VIS-NIR, grating #3, Ocean Optics; Duiven, The Netherlands)(Serôdio et al., 2009). Light was
614 collected using a 400- μm diameter fiber optic (QP400-2-VIS/NIR-BX, Ocean Optics) positioned
615 perpendicularly to a reference white panel (WS-1-SL Spectralon Reference Standard, Ocean
616 Optics) placed in the center of the sampling area of the fluorometer and the projected
617 light field. A spectrum measured in the dark was subtracted to all measured spectra to account for
618 the dark current noise of the spectrometer. Spectra were smoothed using a 10-point moving
619 average filter.

620

621 **Light-response curves**

622 Light-response curves were generated by determining fluorescence parameters F_s and F_m ,
623 for each AOI, each corresponding to a different irradiance level. F_s and F_m were measured by

624 averaging all pixel values of each AOI and averaging the fluorescence intensity during the 2 s
 625 immediately before the saturating pulse, and during 0.6 s during the application of the saturating
 626 pulse (total duration of 800 ms), respectively. The kinetics of fluorescence intensity recorded
 627 immediately before and during the application of each saturating pulse was analyzed for each
 628 measurement using the FluorCam7 software, and the parts of the fluorescence trace showing
 629 effects of the projector's light flickering were not considered for the estimation of F_s or F_m' . For
 630 each AOI (each irradiance level, E), the relative rETR was calculated from the product of E and
 631 the PSII effective quantum yield, $\Delta F/F_m'$ (Genty et al., 1990):

$$632 \quad \text{rETR} = E \frac{F_m' - F_s}{F_m'} = E \Delta F / F_m' \quad (1)$$

634
 635 Fluorescence measurements were also used to calculate the non-photochemical quenching
 636 (NPQ) index, used to quantify the operation of photoprotective and photoinhibitory processes.
 637 NPQ was calculated from the relative difference between the maximum fluorescence measured
 638 in the dark-adapted state, F_m , and upon exposure to light, F_m' :

$$639 \quad \text{NPQ} = \frac{F_m - F_m'}{F_m'} \quad (2)$$

640
 641
 642 For each AOI, F_m was measured at the end of a 20 min dark adaptation prior to light
 643 exposure. Light-response curves were generated by applying a single saturating pulse after a
 644 defined period of light exposure (e.g. 6 min), following a 20 min dark-adaptation period.

645 **Dynamic light response**

646
 647 The potentialities of the method were further tested by characterizing the dynamic light
 648 response, i.e. the variation of the fluorescence light response over time. After a 20 min dark
 649 adaptation, samples were exposed to the light mask and saturating pulses were applied every 2
 650 min. This rationale was also applied to light stress-recovery experiments, during which samples
 651 were subsequently exposed to darkness, to allow the characterization of the recovery after
 652 exposure to the various actinic light intensities. Data was used to calculate light-response curves
 653 and light kinetics (light induction and dark relaxation) of NPQ, as well as the quenching
 654 coefficients partitioning NPQ into constitutive, photoprotective, photoinhibitory components,
 655 following Guadagno et al. (2010).

656 **Light-response curves models**

658 rETR vs E curves were quantitatively described by fitting the model
 659 of Eilers & Peeters (1988), and by estimating the parameters α (the initial slope of the curve),
 660 $rETR_m$ (maximum rETR) and E_k (the light-saturation parameter):

$$661 \quad 662 \quad rETR(E) = \frac{E}{aE^2 + bE + c} \quad (3)$$

663 where

$$664 \quad 665 \quad \alpha = \frac{1}{c}, \quad rETR_m = \frac{1}{b + \sqrt{ac}} \quad \text{and} \quad E_k = \frac{c}{b + \sqrt{ac}} \quad (4)$$

666
 667 Light-response curves of NPQ were described by fitting the model of Serôdio & Lavaud (2011),
 668 and by estimating the parameters NPQ_m (maximum NPQ), E_{50} (irradiance corresponding to half
 669 of NPQ_m) and n (sigmoidicity parameter):

$$670 \quad 671 \quad NPQ(E) = NPQ_m \frac{E^n}{E_{50}^n + E^n} \quad (5)$$

672
 673 The models were fitted using a procedure written in MS Visual Basic and based on MS Excel
 674 Solver. Model parameters were estimated iteratively by minimizing a least-squares function,
 675 forward differencing, and the default quasi-Newton search method (Serôdio and Lavaud, 2011).

676
 677 **Plant material**

678 The applicability of the method was illustrated on intact plant leaves. To compare the
 679 method in samples having distinct light responses, plants acclimated to contrasting light
 680 conditions were used. For high-light acclimated plants, leaves of *Hedera helix* L. (common ivy)
 681 grown under natural conditions were used. Photoperiod and weather conditions were those of
 682 November-December 2012 in Aveiro, Portugal: 10/14 h photoperiod, temperature range of 4-16
 683 °C, relative humidity of 60-80%, precipitation of 100-200 mm, 95-120 insolation hours. For
 684 low-light acclimated plants, leaves of *Ficus benjamina* L. (weeping fig) grown in a greenhouse
 685 during the same time of year were used (average PAR of 20 $\mu\text{mol m}^{-2} \text{s}^{-1}$). All plants were grown
 686 in standard horticultural soil, and watered every two days. These two species were selected also
 687 to illustrate the variability among leaf optical properties potentially affecting the measuring of
 688 fluorescence in closely located illuminated areas (light scattering within the leaf). Unless stated
 689 otherwise, all fluorescence measurements were made in the upper (adaxial) surface of the
 690 leaves.

| | |
|-----|---|
| 691 | List of abbreviations |
| 692 | |
| 693 | α - Initial slope of the rETR vs. E curve |
| 694 | a, b, c – parameters of the Eilers and Peeters (1988) model |
| 695 | AAL – Areas of Actinic Light |
| 696 | AOI – Areas of interest |
| 697 | $\Delta F/F_m'$ – Effective quantum yield of PSII |
| 698 | E – PAR irradiance ($\mu\text{mol photons m}^{-2} \text{s}^{-1}$) |
| 699 | E_{50} – Irradiance level corresponding to 50% of NPQ_m in a NPQ vs. E curve |
| 700 | E_k – Light-saturation parameter of the rETR vs. E curve |
| 701 | rETR – PSII relative electron transport rate |
| 702 | rETR_m – Maximum rETR in a rETR vs. E curve |
| 703 | F_o, F_m – Minimum and maximum fluorescence of a dark-adapted sample |
| 704 | F_s, F_m' – Steady state and maximum fluorescence of a light-adapted sample |
| 705 | F_v/F_m – Maximum quantum yield of PSII |
| 706 | HL – High light |
| 707 | LC – Light-response curve |
| 708 | LL – Low light |
| 709 | n – Sigmoidicity coefficient of the NPQ vs. E curve |
| 710 | NPQ – Non-photochemical quenching index |
| 711 | NPQ_m – Maximum NPQ value reached in a NPQ vs. E curve |
| 712 | PSII – Photosystem II |
| 713 | Φ_{qC} – quantum yield of chlorophyll photophysical decay |
| 714 | Φ_{qE} –quantum yield of energy-dependent quenching |
| 715 | Φ_{qT+qI} – quantum yield of state transition and photoinhibitory quenching |
| 716 | SPLC – Single Pulse Light Curve |
| 717 | |

718 **ACKNOWLEDGEMENTS**

719 We thank Gonçalo Simões for invaluable technical help on testing of digital projectors. This
720 work benefited from discussions with Sónia Cruz, Jorge Marques da Silva, Paulo Cartaxana,
721 and David Suggett.

722

723 **REFERENCES**

724

725 **Eilers PHC, Peeters JCH** (1988) A model for the relationship between light intensity and the
726 rate of photosynthesis in phytoplankton. *Ecol Model* **42**: 199–215

727

728 **Genty B, Briantais JM, Baker NR** (1989) The relationship between the quantum yield of
729 photosynthetic electron transport and quenching of chlorophyll fluorescence.
730 *BiochimBiophysActa* **990**: 87–92

731

732 **Genty B, Harbinson J, Baker NR** (1990) Relative quantum efficiencies of the two
733 photosystems of leaves in photorespiratory and non-photorespiratory conditions. *Plant*
734 *PhysiolBiochem* **28**: 1–10

735

736 **Guadagno CR, Virzo De Santo a, D'Ambrosio N** (2010) A revised energy partitioning
737 approach to assess the yields of non-photochemical quenching
738 components. *BiochimBiophysActa* **1797**: 525–530

739

740 **Henley WJ** (1993) Measurement and interpretation of photosynthetic light-response curves in
741 algae in the context of photoinhibition and diel changes. *J Phycol* **29**: 729–739

742

743 **Herlory O, Richard P, Blanchard GF** (2007) Methodology of light response curves:
744 application of chlorophyll fluorescence to microphytobenthic biofilms. *Mar Biol* **153**: 91–101

745

746 **Ihnken S, Eggert A, Beardall J** (2010) Exposure times in rapid light curves affect
747 photosynthetic parameters in algae. *Aquat Bot* **93**: 185–194

748

749 Imaging-PAM, M-Series Chlorophyll fluorometer, Instrument description and information for
750 users (2009). Heinz Walz GmbH, Effeltrich

751

752 **Johnson ZI, Sheldon TL** (2007) A high-throughput method to measure photosynthesis-
753 irradiance curves of phytoplankton. *LimnolOceanogr Meth* **5**: 417–424

754

755 **Lavaud J, Strzepak RF, Kroth PG** (2007) Photoprotection capacity differs among diatoms:
756 Possible consequences on the spatial distribution of diatoms related to fluctuations in the
757 underwater light climate. *LimnolOceanogr* **52**: 1188–1194

758

759 **Lefebvre S, Mouget J-L, Lavaud J** (2011) Duration of rapid light curves for determining the
760 photosynthetic activity of microphytobenthos biofilm *in situ*. *Aquat Bot* **95**: 1–8
761

762 **Müller P, Li XP, Niyogi KK** (2001) Non-photochemical quenching. A response to excess light
763 energy. *Plant Physiol* **125**: 1558–1566
764

765 **Perkins RG, Mouget JL, Lefebvre S, Lavaud J** (2006) Light response curve methodology and
766 possible implications in the application of chlorophyll fluorescence to benthic diatoms. *Mar*
767 *Biol* **149**: 703–712
768

769 **Ralph PJ, Gademann R** (2005) Rapid light curves: a powerful tool to assess photosynthetic
770 activity. *Aquat Bot* **82**: 222–237
771

772 **Rascher U** (2001) Spatiotemporal variation of metabolism in a plant circadian rhythm: The
773 biological clock as an assembly of coupled individual oscillators. *Proc Natl Acad Sci USA* **98**:
774 11801–11805
775

776 **Rascher U, Liebig M, Lüttge U** (2000) Evaluation of instant light-response curves of
777 chlorophyll fluorescence parameters obtained with a portable chlorophyll fluorometer on site in
778 the field. *Plant Cell Environ* **23**: 1397–1405
779

780 **Roháček K** (2010) Method for resolution and quantification of components of the non-
781 photochemical quenching (q_N). *Photosynth Res* **105**: 101–113
782

783 **Schreiber U, Bilger W, Neubauer** (1994) Chlorophyll fluorescence as a noninvasive indicator
784 for rapid assessment of *in vivo* photosynthesis. In: ED Shulze, MM Caldwell, eds, *Ecophysiology*
785 *of Photosynthesis*. Springer-Verlag, Berlin, pp 49–70
786

787 **Schreiber U, Schliwa U, Bilger W** (1986) Continuous recording of photochemical and
788 nonphotochemical chlorophyll fluorescence quenching with a new type of modulation
789 fluorometer. *Photosynth Res* **10**: 51–62
790

791 **Schreiber U, Gademann R, Ralph PJ, Larkum AWD** (1997) Assessment of photosynthetic
792 performance of *Prochloron* in *Lissoclinum patella* in hospite by chlorophyll fluorescence
793 measurements. *Plant Cell Physiol* **38**: 945–951
794

795 **Schreiber U, Klughammer C, Kolbowski J** (2012) Assessment of wavelength-dependent
796 parameters of photosynthetic electron transport with a new type of multi-color PAM chlorophyll
797 fluorometer. *Photosynth Res* **113**: 127–144
798
799 **Seaton GGR, Walker DA** (1990) Chlorophyll fluorescence as a measure of photosynthetic
800 carbon assimilation. *Proc Royal Soc Lond B* **242**: 29–35
801
802 **Serôdio J, Cartaxana P, Coelho H, Vieira S** (2009) Effects of chlorophyll fluorescence on the
803 estimation of microphytobenthos biomass using spectral reflectance indices. *Rem Sens Environ*
804 **113**: 1760–1768
805
806 **Serôdio J, Ezequiel J, Barnett A, Mouget J, Méléder V, Laviale M, Lavaud J** (2012)
807 Efficiency of photoprotection in microphytobenthos: role of vertical migration and the
808 xanthophyll cycle against photoinhibition. *Aquat Microb Ecol* **67**: 161–175
809
810 **Serôdio J, Lavaud J** (2011) A model for describing the light response of the nonphotochemical
811 quenching of chlorophyll fluorescence. *Photosynth Res* **108**: 61–76
812
813 **Serôdio J, Vieira S, Cruz S, Barroso F** (2005) Short-term variability in the photosynthetic
814 activity of microphytobenthos as detected by measuring rapid light curves using variable
815 fluorescence. *Mar Biol* **146**: 903–914
816
817 **Serôdio J, Vieira S, Cruz S, Coelho H** (2006) Rapid light-response curves of chlorophyll
818 fluorescence in microalgae: relationship to steady-state light curves and non-photochemical
819 quenching in benthic diatom-dominated assemblages. *Photosynth Res* **90**: 29–43
820
821 **Smith EL** (1936) Photosynthesis in relation to light and carbon dioxide. *Proc Natl Acad Sci USA*
822 **22**: 504–511
823
824 **Walters RG, Horton P** (1991) Resolution of components of non-photochemical chlorophyll
825 fluorescence quenching in barley leaves. *Photosynth Res* **27**: 121–133
826
827 **White AJ, Critchley C** (1999) Rapid light curves: a new fluorescence method to assess the
828 state of the photosynthetic apparatus. *Photosynth Res* **59**: 63–72
829

830 **Ye Z-P, Robakowski P, Suggett DJ** (2012) A mechanistic model for the light response of
831 photosynthetic electron transport rate based on light harvesting properties of photosynthetic
832 pigment molecules. *Planta***237**: 837-847
833

834 **Figure legends**

835

836 **Figure 1.** Scheme showing the relative position of the digital projector, the imaging chlorophyll
837 fluorometer components (the CCD camera and the LED panels emitting saturating pulses) the
838 sampling area and the projected actinic light mask (not at scale). For simplicity, two additional
839 LED panels emitting non-actinic, measuring light, positioned perpendicularly to the shown
840 panels, were omitted. Horizontal arrow indicates increasing levels of actinic light in the light
841 mask.

842

843 **Figure 2.** Variation of light spectrum with intensity. A. Spectrum of the light emitted by the
844 digital projector at different output intensities. Numbers represent PAR measured at the sample
845 level ($\mu\text{mol m}^{-2} \text{s}^{-1}$). B. Variation (%) of the light spectrum relatively to the light projecting 150
846 $\mu\text{mol m}^{-2} \text{s}^{-1}$ at the sample level. C. Comparison between the proportion of G:B and R:B for the
847 different PAR levels used for generating light-response curves, before and after spectral
848 correction through manipulation of the RGB code.

849

850 **Figure 3.** Effects of digital projector light flickering (arrows) on the recording of chlorophyll
851 fluorescence immediately prior (for the determination of F_s) and during a saturating pulse (for
852 the determination of F_m'), emitted by a sample exposed to actinic light of 260 and 850 $\mu\text{mol m}^{-2}$
853 s^{-1} . Values normalized to the first measurement.

854

855 **Figure 4.** Example of the application of an actinic light mask on leaves of HL-acclimated
856 *Hedera helix* (A-C) and LL-acclimated *Ficus benjamina* (D-F). Images (false color scale) of F_s
857 (A,D), F_m' (B,E) and $\Delta F/F_m'$ (C,F) measured after 6 min of exposure to the light mask
858 following a period of 20 min in the dark. Fluorescence levels F_s and F_m' normalized to the range
859 of pixel values in each leaf. Scale bar = 1 cm.

860

861 **Figure 5.** 'Single pulse light curves'. Fluorescence light-response curves as generated by the
862 exposure to intact leaves of HL-acclimated *Hedera helix* (A-C) and LL-acclimated
863 *Ficus benjamina* (D-F) to an actinic light mask (data of Fig. 4). Light-response curves (data
864 points) of fluorescence levels F_s and F_m' (A, D), $\Delta F/F_m'$ and rETR (B, E), and NPQ (C, F),
865 fitted models (lines) and estimates of model parameters (Eq. 1 and 2, for rETR and NPQ,
866 respectively).

867

868 **Figure 6.** Dynamic light response. Variation over time of the light response of fluorescence
869 indices $\Delta F/F_m'$ (A, B), rETR (C, D) and NPQ (E, F). Measurements made under selected PAR
870 levels (numbers) as projected by using an actinic light mask on intact leaves of HL-acclimated

871 *Hedera helix* (A, C, E) and LL-acclimated *Ficusbenjamina* (B, D, F) leaves. Light exposure
872 following a 20 min dark exposure. Mean of 3 replicated measurements. Error bars represent ± 1
873 standard error (n=3).

874

875 **Figure 7.**Dynamic light response: light induction of light-response curves.Variation over time
876 of the parameters of the light-response curve of rETR (A-C; parameters of Eq. 1) and NPQ (D-
877 F; parameters of Eq. 2)measure on intact leaves of HL-acclimated *Hedera helix* and LL-
878 acclimated *Ficusbenjamina*upon light exposure following a 20 min dark adaptation.

879

880 **Figure 8.**Dynamic light response: light stress-recovery experiment.3-D representation of the
881 time and light response of NPQ of a LL-acclimated *Ficusbenjamina* leaf, highlighting the
882 variation over time of the light-response curve (A, C) or the light induction and dark relaxation
883 kinetics (B, D). Light exposure following a 20 min dark adaptation.

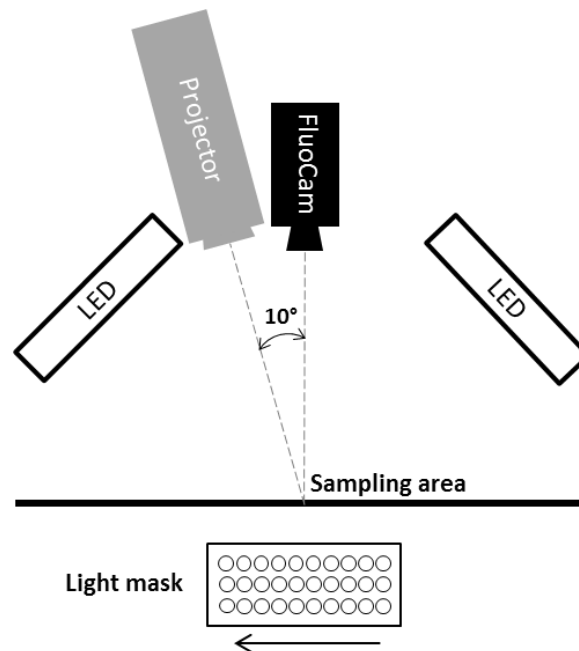
884

885 **Figure 9.**Dynamic light response: quantum yield of NPQ components.Light response of the
886 quantum yield of NPQ components Φ_C , Φ_E , and Φ_{T+I} , as calculated from the data of a light
887 stress-recovery experiment carried on intact leaves of HL-acclimated *Hedera helix*(A) and LL-
888 acclimated *Ficusbenjamina*(B).

889

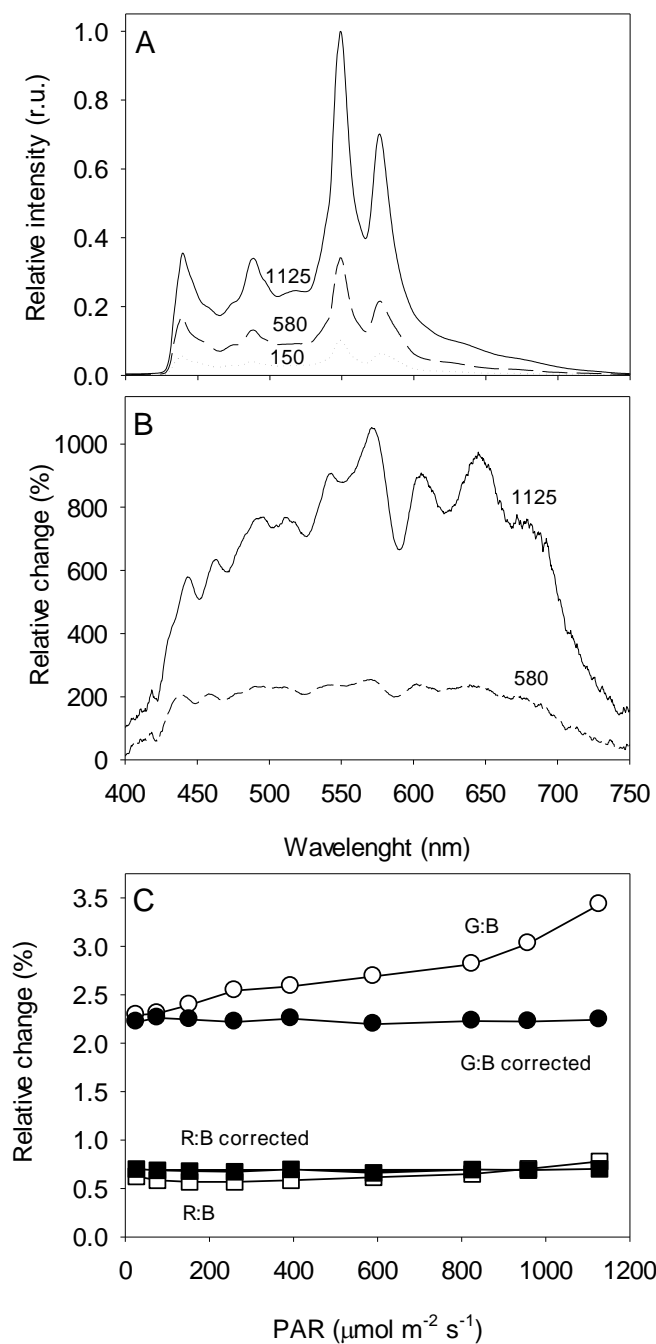
890

891
892
893



894
895
896
897
898
899
900
901
902
903
904

Figure 1. Scheme showing the relative position of the digital projector, the imaging chlorophyll fluorometer components (the CCD camera and the LED panels emitting saturating pulses) the sampling area and the projected actinic light mask (not at scale). For simplicity, two additional LED panels emitting non-actinic, measuring light, positioned perpendicularly to the shown panels, were omitted. Horizontal arrow indicates increasing levels of actinic light in the light mask.



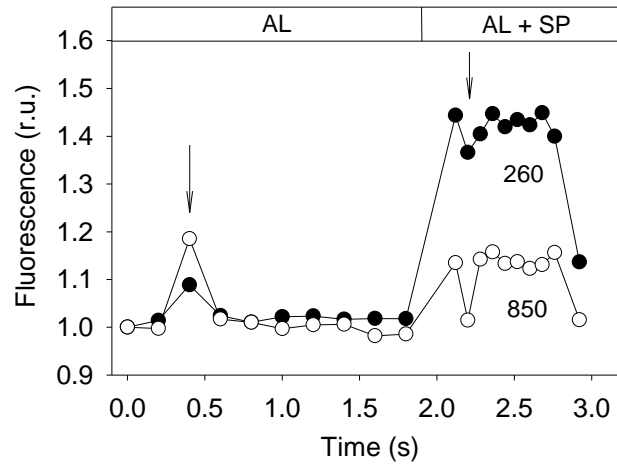
906

907 **Figure 2.** Variation of light spectrum with intensity. A. Spectrum of the light emitted by the
 908 digital projector at different output intensities. Numbers represent PAR measured at the sample
 909 level ($\mu\text{mol m}^{-2} \text{s}^{-1}$). B. Variation (%) of the light spectrum relatively to the light projecting 150
 910 $\mu\text{mol m}^{-2} \text{s}^{-1}$ at the sample level. C. Comparison between the proportion of G:B and R:B for the
 911 different PAR levels used for generating light-response curves, before and after spectral
 912 correction through manipulation of the RGB code.

913

914

915



916

917

918

919

920

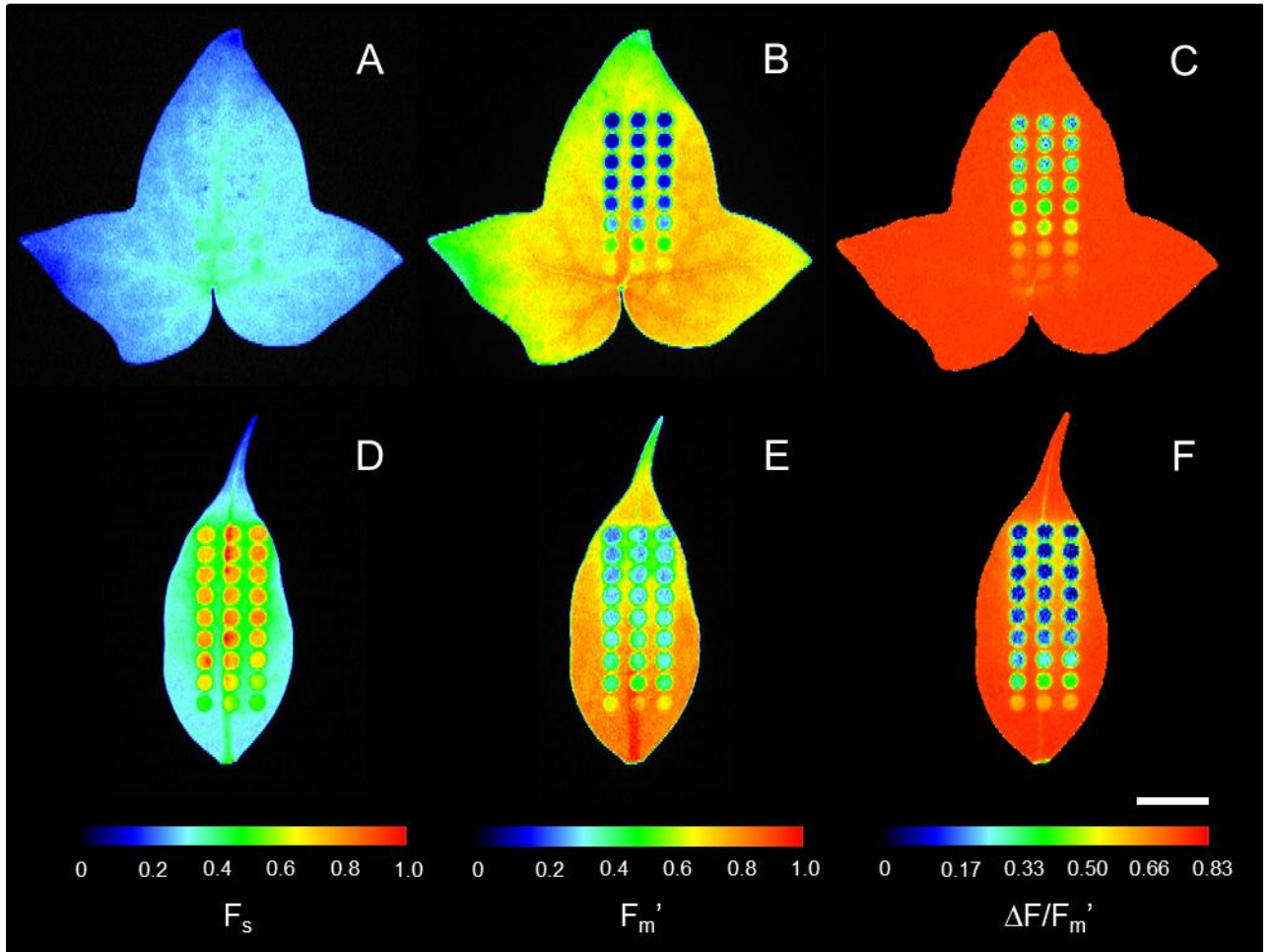
921 **Figure 3.** Effects of digital projector light flickering (arrows) on the recording of chlorophyll
922 fluorescence immediately prior (for the determination of F_s) and during a saturating pulse (for
923 the determination of F_m'), emitted by a sample exposed to actinic light of 260 and 850 $\mu\text{mol m}^{-2}$
924 s^{-1} . Values normalized to the first measurement.

925

926

927

928



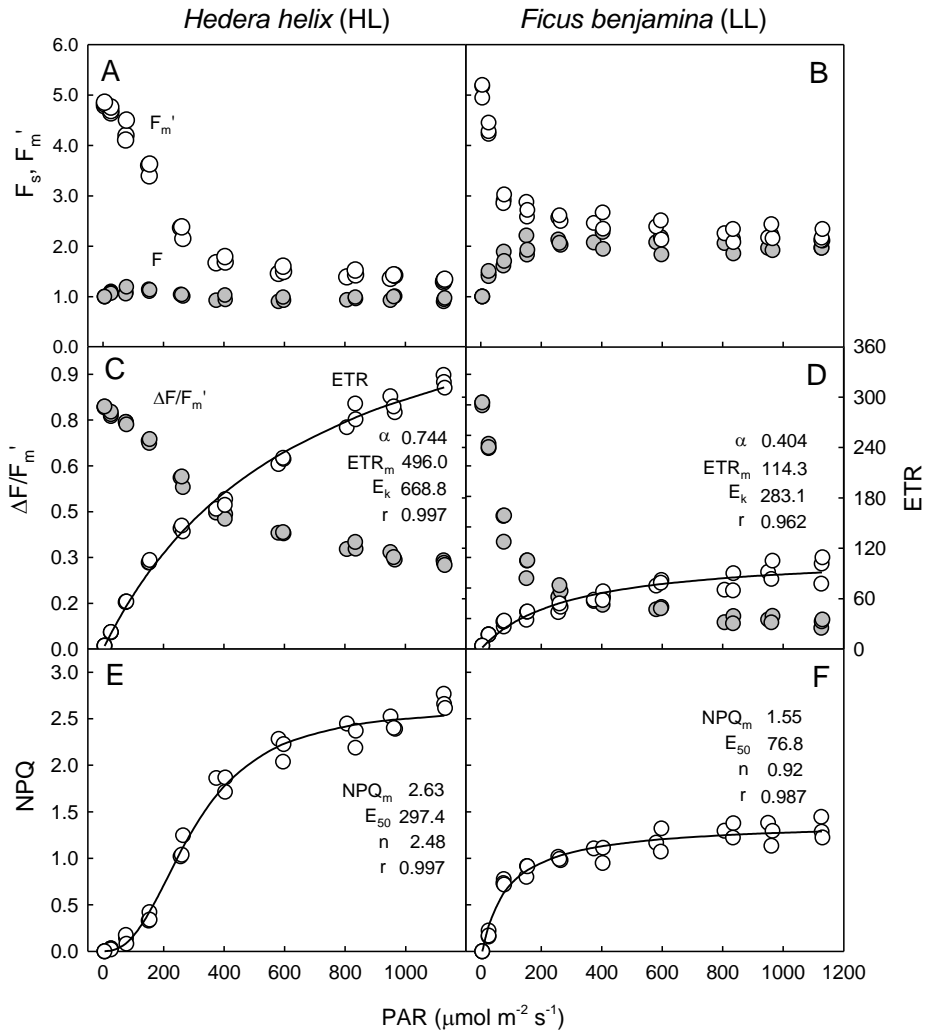
929

930

931

932 **Figure 4.** Example of the application of an actinic light mask on leaves of HL-acclimated
933 *Hedera helix* (A-C) and LL-acclimated *Ficus benjamina* (D-F). Images (false color scale) of F_s
934 (A,D), F_m' (B,E) and $\Delta F/F_m'$ (C,F) measured after 6 min of exposure to the light mask
935 following a period of 20 min in the dark. Fluorescence levels F_s and F_m' normalized to the range
936 of pixel values in each leaf. Scale bar = 1 cm.

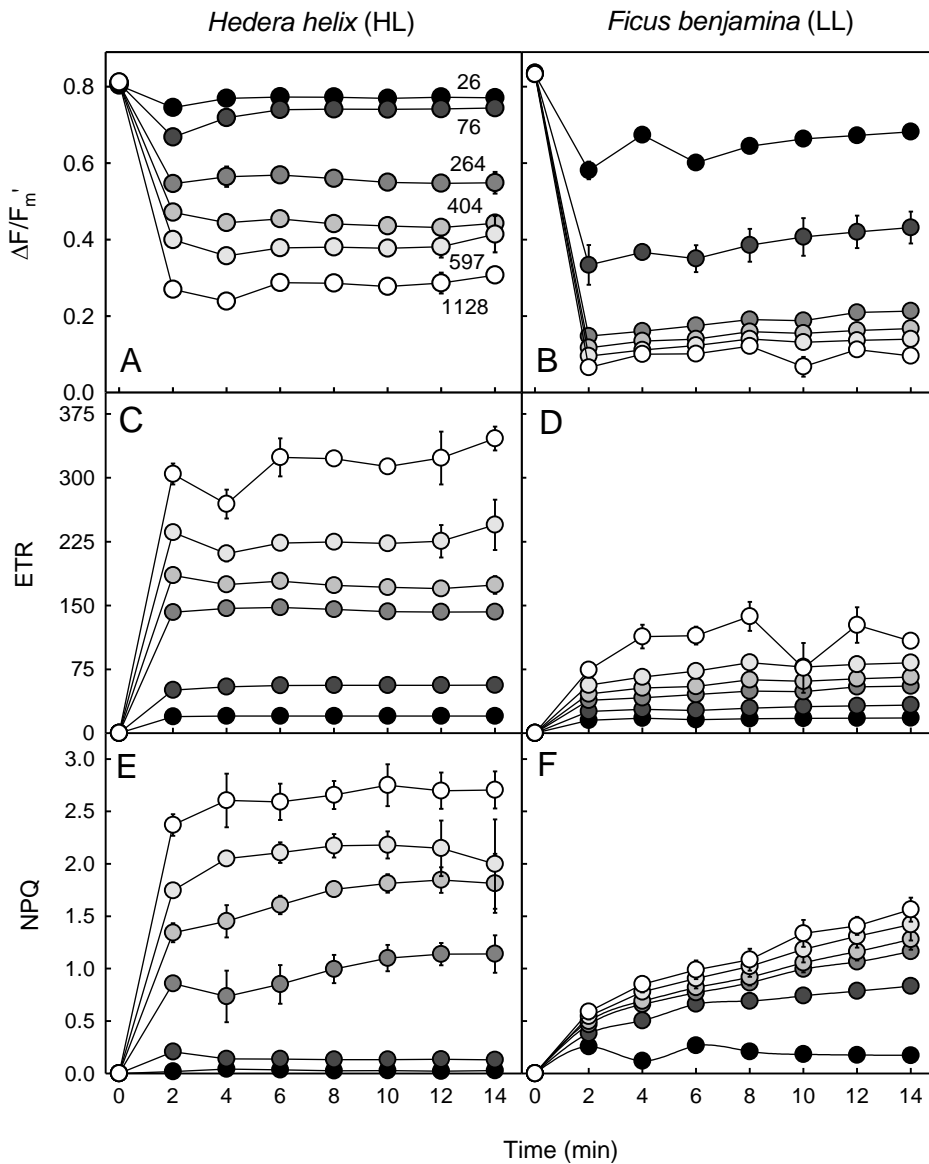
937
 938
 939



940
 941
 942
 943
 944
 945
 946
 947
 948

Figure 5. ‘Single pulse light curves’. Fluorescence light-response curves as generated by the exposure to intact leaves of HL-acclimated *Hedera helix* (A-C) and LL-acclimated *Ficus benjamina* (D-F) to an actinic light mask (data of Fig. 4). Light-response curves (data points) of fluorescence levels F_s and F_m' (A, D), $\Delta F/F_m'$ and rETR (B, E), and NPQ (C, F), fitted models (lines) and estimates of model parameters (Eq. 1 and 2, for rETR and NPQ, respectively).

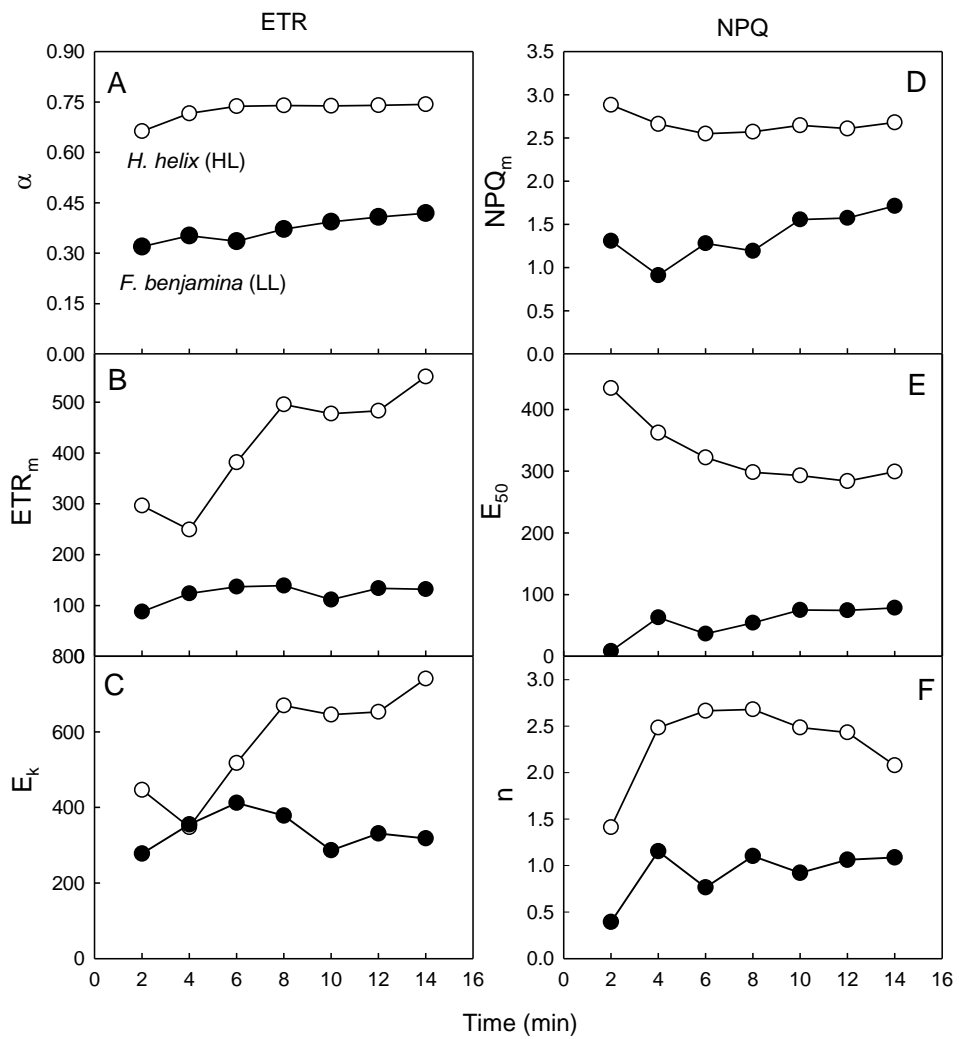
950
951
952



953
954

955 **Figure 6.** Dynamic light response. Variation over time of the light response of fluorescence
956 indices $\Delta F/F_m'$ (A, B), rETR (C, D) and NPQ (E, F). Measurements made under selected PAR
957 levels (numbers) as projected by using an actinic light mask on intact leaves of HL-acclimated
958 *Hedera helix* (A, C, E) and LL-acclimated *Ficus benjamina* (B, D, F) leaves. Light exposure
959 following a 20 min dark exposure. Mean of 3 replicated measurements. Error bars represent ± 1
960 standard error (n=3).

961
 962
 963
 964



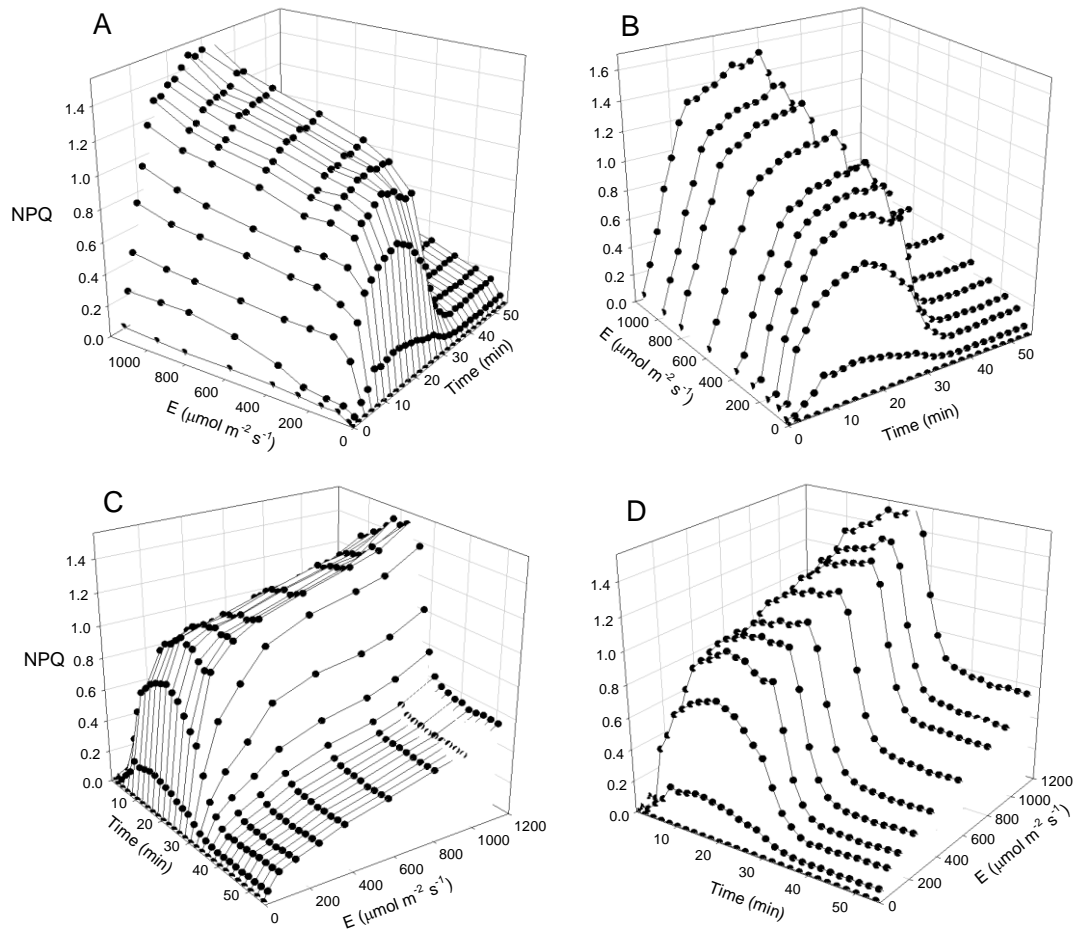
965
 966
 967
 968
 969
 970
 971

Figure 7. Dynamic light response: light induction of light-response curves. Variation over time of the parameters of the light-response curve of rETR (A-C; parameters of Eq. 1) and NPQ (D-F; parameters of Eq. 2) measure on intact leaves of HL-acclimated *Hedera helix* and LL-acclimated *Ficus benjamina* upon light exposure following a 20 min dark adaptation.

972

973

974



975

976

977

978

979

980 **Figure 8.** Dynamic light response: light stress-recovery experiment. 3-D representation of the

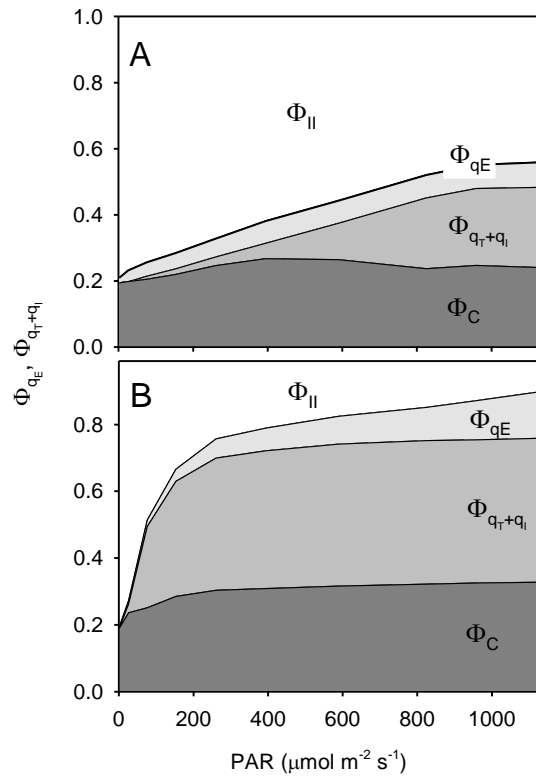
981 time and light response of NPQ of a LL-acclimated *Ficus benjamina* leaf, highlighting the

982 variation over time of the light-response curve (A, C) or the light induction and dark relaxation

983 kinetics (B, D). Light exposure following a 20 min dark adaptation.

984

985
986
987



988
989
990
991
992
993
994
995
996
997

Figure 9. Dynamic light response: quantum yield of NPQ components. Light response of the quantum yield of NPQ components Φ_C , Φ_E , and Φ_{T+I} , as calculated from the data of a light stress-recovery experiment carried on intact leaves of HL-acclimated *Hedera helix* (A) and LL-acclimated *Ficus benjamina* (B).